Structural Studies on Organotransition-metal–Bismuth Complexes†

William Clegg,[a] Neville A. Compton,[a] R. John Errington,[a] George A. Fisher,[a] David C. R. Hockless,[a] Nicholas C. Norman,*[,a] Nicholas A. L. Williams,[b] Susan E. Stratford,[b] Stephen J. Nichols,[b] Penelope S. Jarrett[b] and A. Guy Orpen*[,b]

[a] *Department of Chemistry, The University, Newcastle upon Tyne NE1 7RU, UK*

[b] *Department of Inorganic Chemistry, The University, Bristol BS8 1TS, UK*

The X-ray single-crystal structures are reported for $[BiX\{M(CO)_3(\eta\text{-}C_5H_5)\}_2]$ (M = W, X = Cl **2**; M = Mo, X = Br **3**; M = Mo, X = I **4**). Compounds **2** and **3** exhibit linear polymeric structures involving intermolecular Bi · · · X interactions and are isomorphous with the previously reported $[BiCl\{Mo(CO)_3(\eta\text{-}C_5H_5)\}_2]$ **1**. In contrast, the iodide derivative **4** exists in the solid state as a weakly bound dimer. Analysis of Bi-L_{III}-edge and M-K-edge or L_{III}-edge extended X-ray absorption fine structure (EXAFS) spectra for $[BiCl\{M(CO)_y(\eta\text{-}C_5H_5)\}_2]$ (M = W or Mo; y = 3 **2**, **1**: M = Fe; y = 2 **5**) and $[Bi\{M(CO)_3(\eta\text{-}C_5H_5)\}_3]$ (M = W **6** or Mo **7**) in solid (**1**, **2**, **5**, **7**) and solution (**1**, **5**) phases also shows evidence for oligo- or poly-merisation through Bi · · · Cl interactions in solid **1**, **2** and **5**. In tetrahydrofuran (thf) solutions of **1** and **5** these interactions are disrupted, and the monomeric species formed show co-ordination of solvent to bismuth. The BiM_3 species **6** and **7** show metal–metal distances consistent with a pyramidal geometry at bismuth. EXAFS data for $BiCl_3$ **8** in the solid and in thf solution showed only indirect evidence for disruption of the weaker Bi · · · Cl contacts present in the solid on solvation.

As part of our interest in organotransition-metal–bismuth complexes, we have determined several structures by X-ray crystallography [1–3] and more recently we have examined, in both the solid state and in solution, a number of compounds by extended X-ray absorption fine structure spectroscopy (EXAFS).[4] The latter technique has proven extremely useful in studying structures in the solid state where crystals suitable for X-ray diffraction are not available but, and of perhaps greater importance, it has also enabled us to study the nature of complexes in solution. All of these data provide valuable structural information and, in addition, they often allow us to understand better much of the chemistry of these compounds. Herein we describe further results obtained by X-ray crystallography and EXAFS and comment on the nature of the bismuth centre in these complexes particularly with regard to its Lewis acidity.

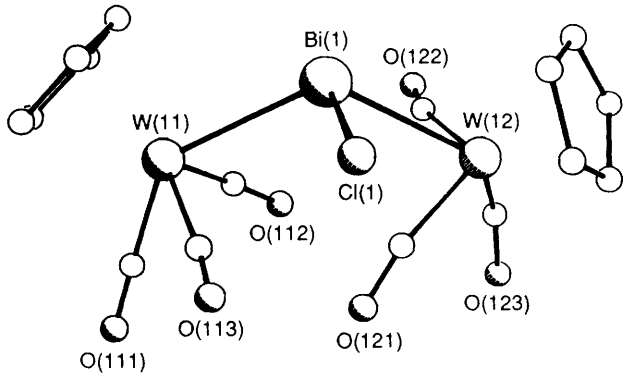

Fig. 1 A view of the molecular structure of molecule **A** of complex **2**. Hydrogen atoms omitted for clarity

Results and Discussion

(*i*) *X-Ray Crystallography.*—In ref. 2 we described the structure of $[BiCl\{Mo(CO)_3(\eta\text{-}C_5H_5)\}_2]$ **1**. Compound **1** crystallises with two molecules, **A** and **B**, in the asymmetric unit; these, although similar in their molecular structures,[2] exhibit large differences in their intermolecular interactions. Thus for **A** substantial Bi · · · Cl interactions exist between adjacent symmetry-related molecules such that, whilst the primary Bi–Cl bond distance is 2.746(2) Å, the secondary, intermolecular distance is only *ca.* 0.29 Å longer at 3.039(3) Å. For molecule **B** much weaker intermolecular interactions are present; the primary Bi–Cl distance is 2.612(3) Å whereas the secondary distance is *ca.* 0.98 Å longer at 3.596(4) Å. These data show that as the secondary Bi · · · Cl distance decreases the primary Bi–Cl distance increases. Moreover, the Cl–Bi–Cl angles [151.6(1)° for **A** and 141.6(1)° for **B**] show that the secondary chlorine interaction is approximately *trans* to the primary Bi–Cl bond. We shall return to and discuss these observations later.

The complexes $[BiCl\{W(CO)_3(\eta\text{-}C_5H_5)\}_2]$ **2** and $[BiBr\{Mo(CO)_3(\eta\text{-}C_5H_5)\}_2]$ **3** are isomorphous with **1**. The synthesis of **2** was described in ref. 2; **3** was prepared in exactly the same way as **1** but using $BiBr_3$, although an alternative preparation of this complex involving the reaction between $Na[Mo(CO)_3(\eta\text{-}C_5H_5)]$ and $BiBrMe_2$ has been reported by Panster and Malisch.[5]

A view of molecule **A** of complex **2** is shown in Fig. 1, selected bond lengths and angles are given in Table 1 and atomic positional parameters in Table 2. For molecule **A** the primary Bi–Cl distance is 2.752(6) Å and the secondary Bi · · · Cl interaction is *ca.* 0.27 Å longer at 3.017(6) Å. For molecule **B** the related distances are 2.604(7) and 3.620(6) Å (the latter 1.02 Å longer). The Cl–Bi–Cl angles are 151.9(4)° for **A** and 141.8(4)° for **B**.

A view of molecule **A** of complex **3** is shown in Fig. 2, selected bond lengths and angles are given in Table 3 and atomic positional parameters in Table 4. The primary and secondary

† *Supplementary data available:* see Instructions for Authors, *J. Chem. Soc., Dalton Trans.*, 1992, Issue 1, pp. xx–xxv.

Bi–Br distances are, for molecule **A**, 2.938(2) and 3.104(2) Å respectively and, for **B**, 2.773(2) and 3.718(2) Å respectively. The Br–Bi–Br angles are, for **A**, 148.2(1)° and, for **B**, 140.7(1)°. A view of part of the unit cell of **3** (Fig. 3) illustrates the intermolecular interactions.

The iodide complex $[BiI\{Mo(CO)_3(\eta\text{-}C_5H_5)\}_2]$ **4**, in contrast to **1**–**3**, is a weakly bound dimer. A view of **4** is shown in Fig. 4 and one of the dimeric units is shown in Fig. 5. Selected bond lengths and angles are given in Table 5 and atomic positional parameters in Table 6. The primary Bi–I bond length is 2.949(1) Å whereas the secondary Bi · · · I interaction is over 1 Å longer at 4.152(1) Å.

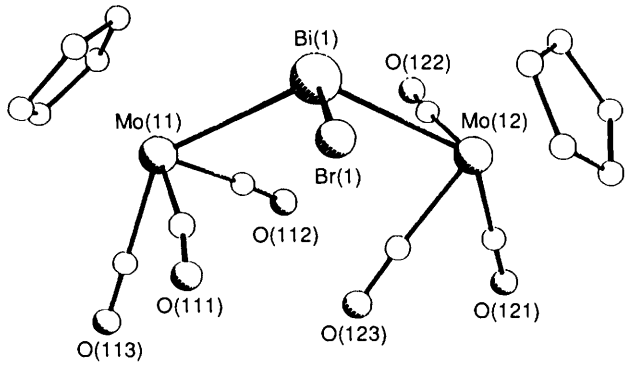

Fig. 2 A view of the molecular structure of molecule **A** of complex **3**. Hydrogen atoms omitted for clarity

(ii) EXAFS.—Transmission EXAFS data were collected on solid samples of complexes **1**, **2**, $[BiCl\{Fe(CO)_2(\eta\text{-}C_5H_5)\}_2]$ **5**, $[Bi\{W(CO)_3(\eta\text{-}C_5H_5)\}_3]$ **6**, $[Bi\{Mo(CO)_3(\eta\text{-}C_5H_5)\}_3]$ **7** and $BiCl_3$ **8** and on tetrahydrofuran (thf) solutions of **1**, **5** and **8** as described in the Experimental section. The results of the EXAFS data analyses are summarised in Table 7. Typical Fourier transform (quasi-radial distribution function) and EXAFS function plots are shown in Figs. 6–8.

For complexes **1** and **5** the principal conclusions to be drawn concern the intramolecular geometry of the $[BiCl\{M(CO)_y(\eta\text{-}C_5H_5)\}_2]$ units, and the Lewis-acid interactions of the bismuth atom, either with the chlorine of another $[BiCl\{M(CO)_y(\eta\text{-}C_5H_5)\}_2]$ moiety or with the oxygen of the solvent. The solid-state structures of **1** and **5** had been known for some time prior to this work [1,2,6] and that of **2**, obtained after the EXAFS work reported in Table 7, is described in the preceding section. The solid-state structures of **1** and **5** as determined by EXAFS are fully consistent with the X-ray determined structures. Thus for **1**

Table 1 Selected bond lengths (Å) and angles (°) for complex **2**

Molecule **A**		Molecule **B**	
Bi(1)–W(11)	2.964(2)	Bi(2)–W(21)	2.915(2)
Bi(1)–W(12)	2.935(1)	Bi(2)–W(22)	2.981(2)
Bi(1)–Cl(1)	2.752(6)	Bi(2)–Cl(2)	2.604(7)
Bi(1) · · · Cl(1b)	3.017(6)	Bi(2) · · · Cl(2d)	3.620(6)
W(11)–Bi(1)–W(12)	117.7(1)	W(21)–Bi(2)–W(22)	115.9(1)
W(11)–Bi(1)–Cl(1)	102.2(2)	W(21)–Bi(2)–Cl(2)	96.3(2)
W(12)–Bi(1)–Cl(1)	91.0(2)	W(22)–Bi(2)–Cl(2)	106.4(2)
W(11)–Bi(1)–Cl(1b)	95.7(2)	W(21)–Bi(2)–Cl(2d)	86.8(2)
W(12)–Bi(1)–Cl(1b)	99.8(2)	W(22)–Bi(2)–Cl(2d)	106.3(2)
Cl(1)–Bi(1)–Cl(1b)	151.9(4)	Cl(2)–Bi(2)–Cl(2d)	141.8(4)
Bi(1)–Cl(1)–Bi(1a)	147.6(1)	Bi(2)–Cl(2)–Bi(2c)	136.5(1)

Symmetry operations: a $\frac{3}{2} - x, -\frac{1}{2} + y, \frac{1}{2} - z$; b $\frac{3}{2} - x, \frac{1}{2} + y, \frac{1}{2} - z$; c $\frac{1}{2} - x, \frac{1}{2} + y, \frac{1}{2} - z$; d $\frac{1}{2} - x, -\frac{1}{2} + y, \frac{1}{2} - z$.

Table 3 Selected bond lengths (Å) and angles (°) for complex **3**

Molecule **A**		Molecule **B**	
Bi(1)–Mo(11)	2.963(1)	Bi(2)–Mo(21)	2.987(1)
Bi(1)–Mo(12)	2.939(1)	Bi(2)–Mo(22)	2.927(1)
Bi(1)–Br(1)	2.938(2)	Bi(2)–Br(2)	2.773(2)
Bi(1) · · · Br(1b)	3.104(2)	Bi(2) · · · Br(2d)	3.718(2)
Mo(11)–Bi(1)–Mo(12)	118.9(1)	Mo(21)–Bi(2)–Mo(22)	116.2(1)
Mo(11)–Bi(1)–Br(1)	102.3(1)	Mo(21)–Bi(2)–Br(2)	107.3(1)
Mo(12)–Bi(1)–Br(1)	91.9(1)	Mo(22)–Bi(2)–Br(2)	96.8(1)
Mo(11)–Bi(1)–Br(1b)	98.5(1)	Mo(21)–Bi(2)–Br(2d)	105.4(1)
Mo(12)–Bi(1)–Br(1b)	99.0(1)	Mo(22)–Bi(2)–Br(2d)	87.7(1)
Br(1)–Bi(1)–Br(1b)	148.2(1)	Br(2)–Bi(2)–Br(2d)	140.7(1)
Bi(1)–Br(1)–Bi(1a)	142.2(1)	Bi(2)–Br(2)–Bi(2c)	132.6(1)

Symmetry operations: a $\frac{1}{2} - x, -\frac{1}{2} + y, \frac{3}{2} - z$; b $\frac{1}{2} - x, \frac{1}{2} + y, \frac{3}{2} - z$; c $\frac{1}{2} - x, -\frac{1}{2} + y, \frac{1}{2} - z$; d $\frac{1}{2} - x, \frac{1}{2} + y, \frac{1}{2} + z$.

Table 2 Atomic coordinates (× 10^4) for complex **2**

Atom	*x*	*y*	*z*	Atom	*x*	*y*	*z*
Bi(1)	7210(1)	1759(1)	2680(1)	Bi(2)	2501(1)	3253(1)	3062(1)
W(11)	7352(1)	1744(1)	4213(1)	W(21)	1030(1)	2154(1)	2890(1)
W(12)	5741(1)	2301(1)	1759(1)	W(22)	3498(1)	3128(1)	4502(1)
Cl(1)	7050(5)	−740(5)	2351(4)	Cl(2)	2054(5)	5561(6)	2870(5)
C(111)	6666(15)	1487(23)	4794(14)	C(211)	1716(14)	872(20)	3275(14)
O(111)	6280(15)	1338(21)	5166(14)	O(211)	2106(15)	16(17)	3509(10)
C(112)	6559(16)	2967(22)	3846(13)	C(212)	1114(16)	3421(21)	3649(15)
O(112)	6083(13)	3669(17)	3685(13)	O(212)	1096(14)	4202(16)	4037(11)
C(113)	6917(14)	74(24)	3910(13)	C(213)	565(16)	1343(23)	3583(11)
O(113)	6680(13)	−895(15)	3863(10)	O(213)	283(13)	889(21)	3957(11)
C(114)	8529(12)	2546(23)	4199(10)	C(214)	790(12)	1275(16)	1783(11)
C(115)	8297	3219	4729	C(215)	1071	2492	1723
C(116)	8227	2359	5258	C(216)	564	3367	1888
C(117)	8416	1154	5055	C(217)	−30	2690	2049
C(118)	8603	1270	4400	C(218)	109	1397	1984
C(121)	5567(16)	1295(23)	2525(16)	C(221)	2561(21)	2214(22)	4580(12)
O(121)	5394(11)	691(19)	2946(12)	O(221)	2114(13)	1663(16)	4742(10)
C(122)	6075(18)	3972(21)	2180(16)	C(222)	3410(17)	3561(21)	5501(15)
O(122)	6183(10)	4951(15)	2330(12)	O(222)	3355(15)	3778(19)	5982(10)
C(123)	4807(18)	2995(24)	1914(18)	C(223)	3217(25)	4900(24)	4380(15)
O(123)	4278(14)	3371(18)	2032(16)	O(223)	3132(19)	5969(16)	4410(11)
C(124)	5372(16)	2686(21)	554(10)	C(224)	4404(16)	1613(22)	4874(15)
C(125)	5074	1519	693	C(225)	4097	1481	4142
C(126)	5677	685	939	C(226)	4280	2567	3806
C(127)	6347	1336	952	C(227)	4701	3370	4330
C(128)	6158	2573	714	C(228)	4778	2780	4990

Table 4 Atomic coordinates (× 10^4) for complex **3**

Atom	x	y	z	Atom	x	y	z
Bi(1)	2816(1)	6639(1)	7273(1)	Bi(2)	2517(1)	6724(1)	1914(1)
Mo(11)	2658(1)	6727(1)	5753(1)	Mo(21)	1513(1)	6876(1)	487(1)
Mo(12)	4262(1)	7250(1)	8210(1)	Mo(22)	3979(1)	7869(1)	2109(1)
Br(1)	3038(1)	4020(1)	7575(1)	Br(2)	3018(1)	4334(1)	2114(1)
C(111)	3123(6)	5110(11)	6014(6)	C(211)	2429(6)	7731(11)	402(5)
O(111)	3389(5)	4159(8)	6071(5)	O(211)	2894(4)	8281(8)	262(4)
C(112)	3447(6)	7930(11)	6136(5)	C(212)	1762(7)	5116(11)	588(6)
O(112)	3910(5)	8656(8)	6308(5)	O(212)	1832(6)	4075(8)	569(5)
C(113)	3329(6)	6542(10)	5124(6)	C(213)	1603(6)	6466(11)	−465(6)
O(113)	3714(6)	6393(9)	4769(5)	O(213)	1674(6)	6267(10)	−1009(5)
C(114)	1702(9)	8133(14)	5319(12)	C(214)	308(8)	6697(14)	659(11)
C(115)	1777(7)	7376(19)	4785(7)	C(215)	256(7)	7262(16)	36(9)
C(116)	1583(7)	6185(14)	4937(9)	C(216)	594(8)	8314(15)	158(10)
C(117)	1403(7)	6247(17)	5564(10)	C(217)	888(8)	8474(19)	849(11)
C(118)	1456(9)	7402(27)	5778(9)	C(218)	701(9)	7460(23)	1169(8)
C(121)	5186(6)	7987(11)	8065(6)	C(221)	3244(5)	9151(10)	1722(5)
O(121)	5720(5)	8403(9)	7981(6)	O(221)	2846(5)	9946(8)	1495(5)
C(122)	3907(6)	8883(10)	7829(6)	C(222)	4457(6)	8689(11)	1433(6)
O(122)	3769(5)	9858(7)	7676(5)	O(222)	4729(5)	9148(9)	1050(5)
C(123)	4474(5)	6259(9)	7438(6)	C(223)	3921(5)	6598(11)	1385(6)
O(123)	4659(5)	5734(9)	7009(5)	O(223)	3953(6)	5897(10)	968(5)
C(124)	4595(10)	7567(17)	9398(7)	C(224)	3955(7)	7570(14)	3273(6)
C(125)	3797(10)	7459(17)	9194(8)	C(225)	4203(8)	8709(13)	3229(6)
C(126)	3651(7)	6235(14)	8968(7)	C(226)	4881(8)	8632(13)	3044(7)
C(127)	4333(8)	5662(14)	9022(7)	C(227)	5039(6)	7417(15)	2966(6)
C(128)	4909(8)	6463(15)	9277(7)	C(228)	4438(7)	6699(13)	3116(6)

Table 5 Selected bond lengths (Å) and angles (°) for complex **4**

Bi–Mo(1)	2.963(1)	Bi–Mo(2)	2.928(1)
Bi–I	2.949(1)	Bi···I′	4.152(1)
Mo(1)–Bi–Mo(2)	118.2(1)	Mo(1)–Bi–I	101.8(1)
Mo(2)–Bi–I	103.2(1)	I–Bi–I′	95.2(1)
Bi–I–Bi′	84.8(1)		

Symmetry operation for primed atoms: $-x, 1-y, 2-z$.

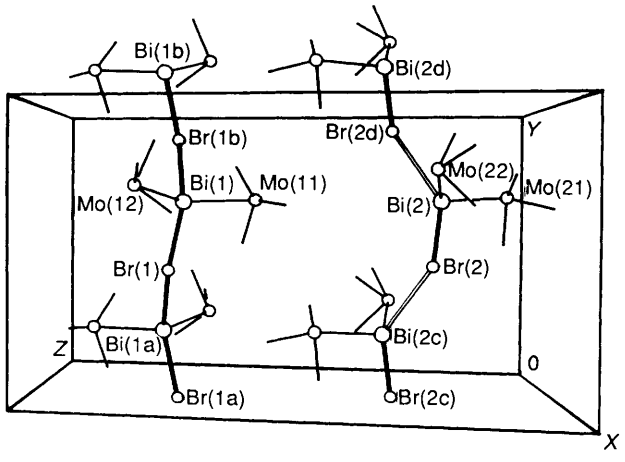

Fig. 3 A view of part of the crystal structure of complex **3** showing the intermolecular Bi···Br contacts. Each $Mo(CO)_3(C_5H_5)$ fragment is represented as a circle and three lines to the carbonyl carbons. The cyclopentadienyl ligands are omitted for clarity

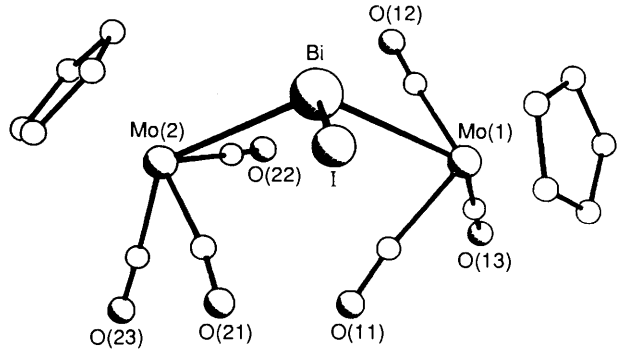

Fig. 4 A view of the molecular structure of complex **4**. Hydrogen atoms omitted for clarity

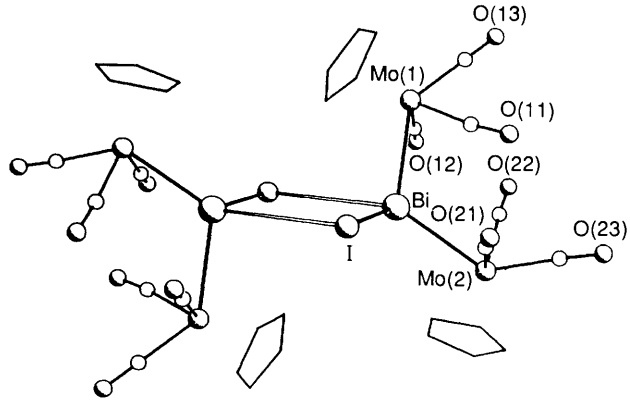

Fig. 5 A view of the dimeric unit in the crystal structure of complex **4**

the crystallographic Bi–Mo distances range from 2.921(1) to 2.983(1) Å (mean 2.951 Å) *cf.* 2.951(3) Å by EXAFS (N.B. the phase shifts for Mo were adjusted to obtain this fit). The Bi···Cl distances in the crystal were 2.612(3), 2.746(2), 3.039(3) and 3.596(4) Å and those by EXAFS 2.599(8), 2.689(5) and 3.41(11) Å although it was not possible to refine four separate Bi···Cl separations. Of these distances only the second EXAFS Bi···Cl contact differs significantly from the X-ray values being 0.057 Å shorter than the lower crystallographic value. This discrepancy arises at least in part because of the similarity of these Bi···Cl and Bi–Mo distances and the consequent overlaps in this region of the quasi-radial distribution function. The possibility of accuracy substantially below precision for such overlapping shells is one that must be

Table 6 Atomic coordinates (× 10^4) for complex **4**

Atom	*x*	*y*	*z*
Bi	417(1)	5353(1)	8500(1)
I	159(1)	6983(1)	9807(1)
Mo(1)	−2078(1)	5165(1)	6918(1)
C(11)	−1389(8)	6327(7)	6467(7)
O(11)	−1102(8)	7022(7)	6132(8)
C(12)	−1134(8)	3938(8)	6898(8)
O(12)	−646(8)	3217(6)	6877(9)
C(13)	−2711(9)	4955(10)	5420(8)
O(13)	−3087(9)	4829(11)	4556(7)
C(14)	−3103(9)	4382(9)	7819(9)
C(15)	−3962(8)	4700(9)	6856(8)
C(16)	−3897(9)	5763(10)	6861(10)
C(17)	−3003(10)	6067(8)	7796(9)
C(18)	−2519(8)	5218(9)	8382(7)
Mo(2)	2272(1)	6131(1)	7874(1)
C(21)	1306(10)	7360(7)	7883(9)
O(21)	876(9)	8112(5)	7894(9)
C(22)	1273(8)	5195(8)	6749(7)
O(22)	789(8)	4636(9)	6094(6)
C(23)	2181(11)	6893(8)	6643(10)
O(23)	2176(13)	7355(9)	5957(10)
C(24)	4021(8)	5157(9)	8435(10)
C(25)	4363(9)	6152(10)	8477(9)
C(26)	4088(9)	6664(8)	9176(8)
C(27)	3549(8)	5987(8)	9600(8)
C(28)	3507(8)	5057(8)	9185(10)

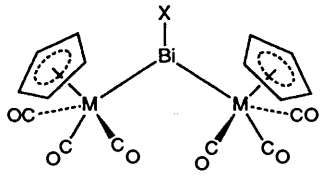

M = Mo, X = Cl **1**; M = W, X = Cl **2**
M = Mo, X = Br **3**; M = Mo, X = I **4**

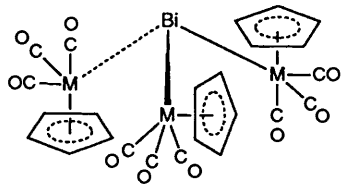

M = W **6** or Mo **7**

taken seriously in several of the studies reported here. As a consequence, some of the distances reported must be viewed with caution. Nevertheless significant qualitative conclusions may safely be drawn as we shall see, even if some quantitative aspects of these results have to be taken less seriously. The Mo-K-edge data for **1** are in reasonable agreement with both the Bi-L_{III} EXAFS and the crystallographic values [Mo–Bi 2.933(2), Mo–C(O) 1.992(3), Mo–C(C_5H_5) 2.367(4), Mo···O 3.139(8) and Mo···Mo 5.05(2) Å]. The latter dimension implies a Mo–Bi–Mo angle of 119(1)° in good agreement with the crystal structure values [118.3(1) and 116.4(1)°].

On dissolution of complex **1** in thf significant changes occur in the EXAFS spectrum (see Fig. 7), especially in the range k = 5–8 $Å^{-1}$. In the model fitting these changes can be seen to be associated with the contraction of the Bi–Cl distance [to 2.551(7) Å] and the disappearance of the long Bi···Cl contact, together with the appearance of a Bi–O contact [2.23(4) Å] associated with a shoulder on the low r side of the main peak in the Fourier transform at *ca.* 3 Å [see Fig. 7(*b*)]. While the length of the Bi–O contact should not be taken too seriously the

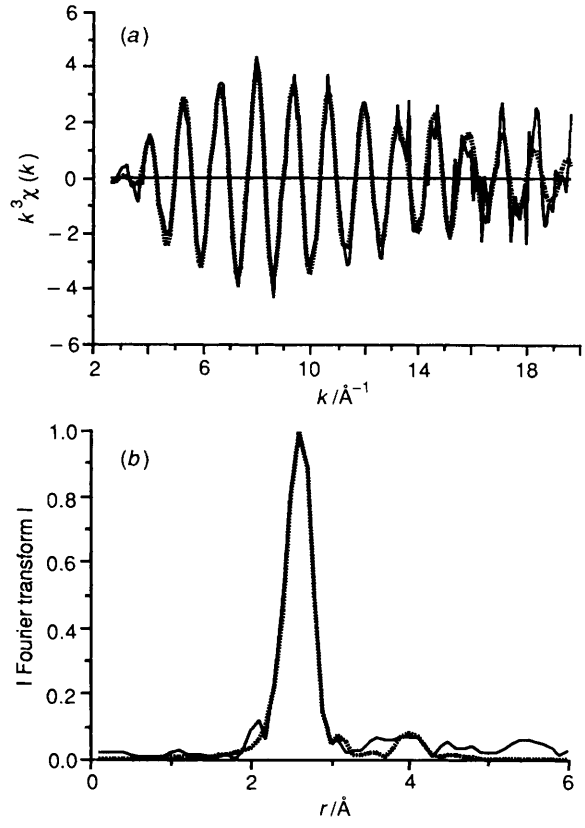

Fig. 6 (*a*) Observed (———) and calculated (– – – –) k^3-weighted Bi-L_{III}-edge EXAFS spectra for complex **5** as a solid at low temperature. (*b*) Observed (——) and calculated (– – – –) Fourier transform magnitudes (quasi-radial distribution function) of (*a*)

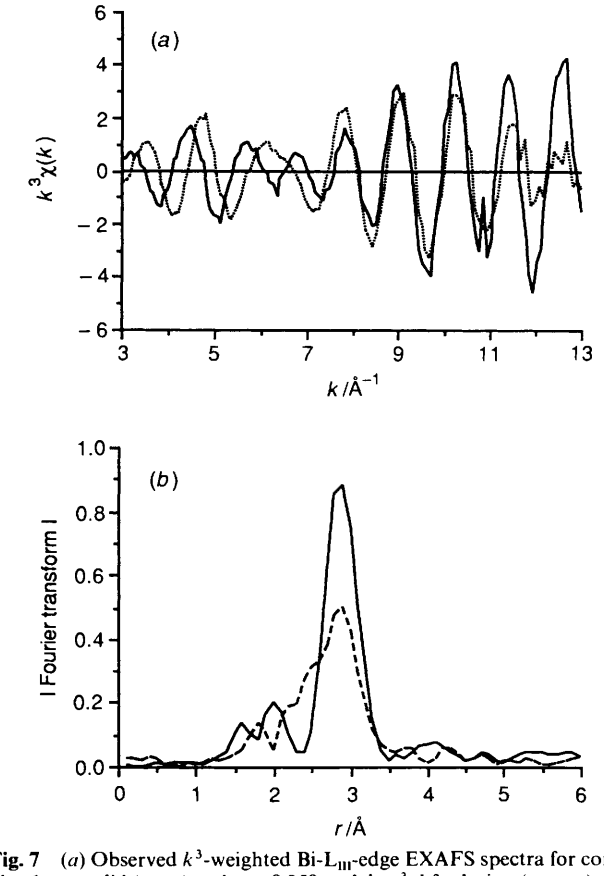

Fig. 7 (*a*) Observed k^3-weighted Bi-L_{III}-edge EXAFS spectra for complex **1** as a solid (——) and as a 0.050 mol dm^{-3} thf solution (– – – –). (*b*) Fourier transform magnitudes (quasi-radial distribution function) of (*a*)

Table 7 EXAFS analyses for $[BiCl_x\{M(CO)_y(\eta\text{-}C_5H_5)\}_{3-x}]$ ($x = 3$; $x = 1$ or 0, $y = 3$, M = W or Mo; $x = 1$, $y = 2$, M = Fe) complexes[a]

Compound	k_{max}/Å^{-1}	R	R'	Shell number (n)[b] 1 Bi–M ($N = 2$)[c]	2 Bi–Cl ($N = 1$)	3 Bi···Cl ($N = 1$)	4 Bi···Bi ($N = 2$)	5 Bi···C ($N = 4$)	6 Bi···O ($N = 1$)	7
Bi-L_{III}-edge data										
2 $[BiCl\{W(CO)_3(\eta\text{-}C_5H_5)\}_2]$										
solid l.t.[d]	15.9	0.10	0.06	2.958(3)	2.688(6)	3.167(8)	3.870(10)	3.397(11)	—	
				0.008(3)	0.008(2)	0.009(2)	0.019(3)	0.043(5)		
		$r_1:r_3$ 0.68; $a_1:a_2$ 0.89, $a_3:a_1$ 0.69, $E_0:r_1$ −0.89, $E_0:r_2$ −0.83, $E_0:r_4$ −0.56, $E_0:r_5$ −0.71								
					($N = 0.5$)					Bi–Cl ($N = 0.5$)
1 $[BiCl\{Mo(CO)_3(\eta\text{-}C_5H_5)\}_2]$										
solid l.t.	17.6	0.12	0.06	2.951(3)	2.599(8)	3.41(11)	—	3.36(4)	—	2.689(5)
				0.006(1)	0.007(2)	0.027(3)		0.023(2)		0.010(1)
		$E_0:r_1$ −0.87, $a_5:r_3$ 0.79, $a_5:a_3$ −0.92, $a_4:r_3$ −0.59, $a_5:r_5$ −0.55, $a_7:r_7$ −0.59, $a_7:a_2$ 0.80								
solution[d] 50 mmol dm^{-3}	19.0	0.21	0.13	2.944(5)	2.551(7)	—	—	2.93(4)	2.23(4)	
				0.016(1)	0.011(1)			0.047(7)	0.048(17)	
		$E_0:r_1$ −0.91, $E_0:r_2$ −0.66, $E_0:r_6$ −0.73, $r_2:r_1$ 0.52, $r_6:r_1$ 0.74, $a_6:r_1$ 0.54, $a_6:r_2$ 0.51								
5 $[BiCl\{Fe(CO)_2(\eta\text{-}C_5H_5)\}_2]$										
solid l.t.	19.8	0.11	0.05	2.689(2)	2.939(4)	3.077(9)	3.985(12)	3.36(10)	—	
				0.007(1)	0.004(1)	0.012(2)	0.019(3)	0.110(22)		
		$E_0:r_1$ −0.83								
										Bi–O ($N = 1$)
solution 64 mmol dm^{-3}	13.0	0.05	0.03	2.761(2)	2.426(18)	—	—	3.280(9)	2.373(3)	3.451(5)
				0.018(2)	0.062(12)			0.027(3)	0.007(1)	0.003(1)
		$E_0:r_1$ −0.80, $a_2:r_1$ 0.54, $a_1:r_2$ −0.55, $E_0:r_5$ −0.71, $a_2:r_6$ −0.61								
6 $[Bi\{W(CO)_3(\eta\text{-}C_5H_5)\}_3]$		($N = 3$)								
solid l.t.	18.3	0.23	0.19	3.002(3)						
				0.009(3)						
		$E_0:r_1$ −0.86								
					Bi–Mo					
7 $[Bi\{Mo(CO)_3(\eta\text{-}C_5H_5)\}_3]$					($N = 1$)			($N = 3$)		
solid l.t.	18	0.32	0.14	3.008(5)	2.884(9)	—	—	3.301(11)		
				0.005(1)	0.008(1)	—	—	0.008(2)		
		$r_1:r_5$ 0.86, $r_1:r_2$ 0.54, $a_5:a_1$ 0.78, $E_0:r_1$ −0.89, $E_0:r_5$ −0.65, $E_0:a_2$ 0.58, $E_0:a_5$ −0.62								
8 $BiCl_3$					($N = 3$)					
solid l.t.	19.0	0.24	0.16	—	2.505(4)					
					0.015(2)					
		$E_0:r_2$ −0.86								
solution 300 mmol dm^{-3}	17.0	0.06	0.03	2.489(1)						
				0.008(1)						
W-L_{III}-edge data				W–Bi ($N = 1$)	W–C ($N = 3$)	W–C ($N = 5$)	W···O ($N = 3$)	W···W[e] ($N = 2$)		
2 $[BiCl\{W(CO)_3(\eta\text{-}C_5H_5)\}_2]$										
solid l.t.	16.0	0.22	0.15	2.923(2)	1.996(4)	2.321(5)	3.114(9)			
				0.005(1)	0.007(1)	0.007(1)	0.012(1)			
6 $[Bi\{W(CO)_3(\eta\text{-}C_5H_5)\}_3]$										
solid l.t.	18.4	0.12	0.08	2.946(4)	1.960(3)	2.330(4)	3.095(5)	4.55(10)		
				0.008(1)	0.005(1)	0.009(1)	0.008(1)	0.04(3)		
Mo-K-edge data										
				Mo–Bi ($N = 1$)	Mo–C ($N = 3$)	Mo–C ($N = 5$)	Mo···O ($N = 3$)	Mo···Mo ($N = 1$)		
1 $[BiCl\{Mo(CO)_3(\eta\text{-}C_5H_5)\}_2]$										
solid l.t.	19.0	0.15	0.11	2.933(2)	1.992(3)	2.367(4)	3.139(8)	5.05(2)		
				0.006(1)	0.004(1)	0.005(2)	0.009(1)	0.015(2)		
7 $[Bi\{Mo(CO)_3(\eta\text{-}C_5H_5)\}_3]$										
solid l.t.	18.0	0.22	0.12	2.940(3)	1.989(3)	2.347(6)	3.126(9)			
				0.008(1)	0.004(1)	0.012(1)	0.016(1)			

Table 7 *continued*

Compound	k_{max}/Å^{-1}	R	R'	Shell number (n)[b] 1 Fe–Bi (N = 1)	2 Fe–C (N = 2)	3 Fe–C (N = 5)	4 Fe···O (N = 2)	5 Fe···Fe (N = 1)	6	7
Fe-K-edge data										
5 $[BiCl\{Fe(CO)_2(\eta\text{-}C_5H_5)\}_2]$										
solid l.t.	17.6	0.32	0.26	2.685(5)	1.750(6)	2.106(6)	2.915(5)	4.318(11)		
				0.008(2)	0.006(1)	0.006(1)	0.010(3)	0.009(3)		
solution 64 mmol dm^{-3}	16.0	0.06	0.05	2.636(5)	1.766(2)	2.098(2)	2.896(4)	—		
				0.013(2)	0.008(1)	0.008(2)	0.010(1)	—		

[a] The estimated standard deviation in the least significant digit as calculated by EXCURV 90 model fitting is given in parentheses, here and throughout this paper. We note that such estimates of precision are likely to be underestimates of accuracy and particularly so in cases of high correlation between parameters (see footnote *b* below). Residual index R was calculated as

$$R = \sum_i \left\{k^3(\chi^{obs}{}_i - \chi^{calc}{}_i)\right\}^2 \Big/ \sum_i \left\{k^3\chi^{obs}{}_i\right\}^2;$$

R' was calculated as for R, with final model parameters, but with data Fourier filtered with r_{max} = *ca.* 6–7 Å to remove noise. [b] For each shell n the distance (r_n in Å) is given above the Debye–Waller factor (a_n in Å^2); correlation coefficients >0.5 between E_0, r_n and a_n are listed below the parameter values. E_0 is the refined correction to the threshold energy of the absorption edge. [c] 'Co-ordination' numbers, N (*i.e.* the number of contacts in a given shell) as assigned (on chemical grounds) are given below the appropriate contact. [d] All solution spectra were measured in thf at ambient temperature (298 K) for the given concentration; low-temperature (l.t.) spectra were measured at liquid-nitrogen temperature (78 K). [e] This shell significant at the 95% level only.

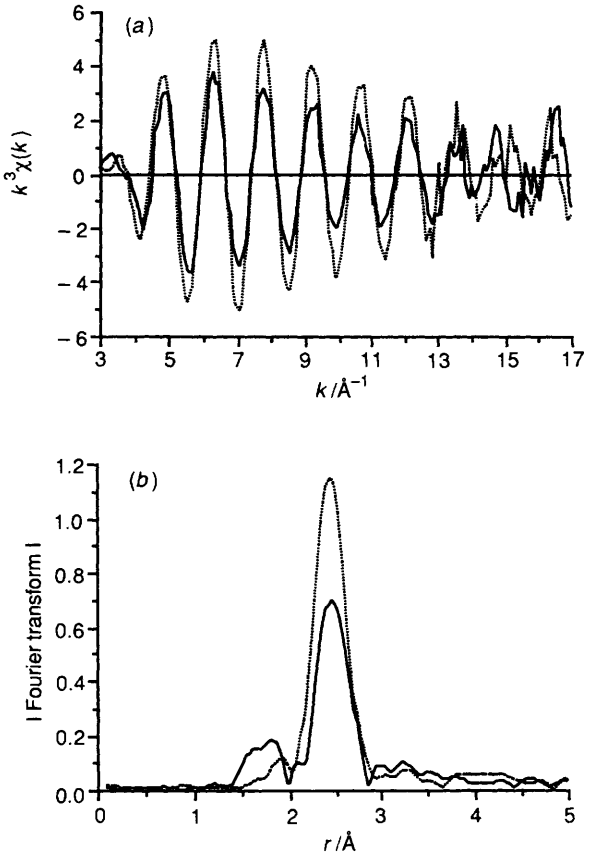

Fig. 8 (*a*) Observed k^3-weighted Bi-L_{III}-edge EXAFS spectra for $BiCl_3$ **8** as a solid (——) and as a 0.30 mol dm^{-3} thf solution (– – – –). (*b*) Fourier transform magnitudes (quasi-radial distribution function) of (*a*)

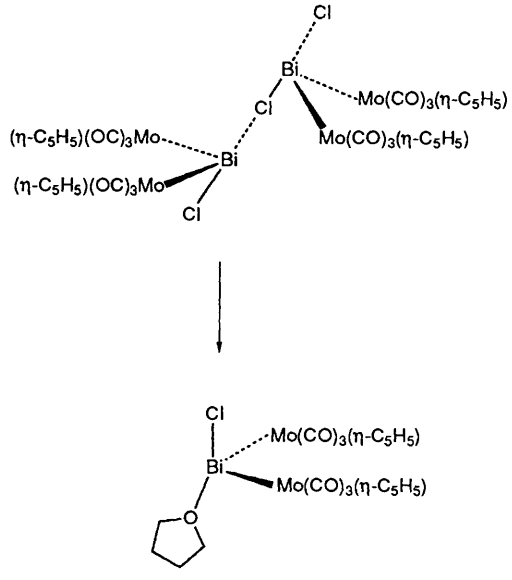

Scheme 1

cumulative evidence for the dissociation (*i.e.* disruption of the Bi–Cl···Bi chains) and solvation of the $[BiCl\{Mo(CO)_3(\eta\text{-}C_5H_5)\}_2]$ monomers is strong (Scheme 1). This behaviour is very similar to that noted for $[BiCl\{Mn(CO)_5\}_2]$[4] and for **5** below. It is particularly noteworthy that while the EXAFS in the region k = 8–11 Å^{-1} is very similar for **1** in solid and solution, it is in the low k region, where O is a strong back-scatterer, that the most dramatic changes are to be seen. In the medium k region where the metal (and chlorine) back scattering would be expected to be dominant there is little change on dissolution, reflecting the maintenance of the Bi–Cl and Bi–Mo co-ordination sphere. At high k the higher temperature at which the solution spectra were acquired is reflected in the decreased amplitude of the EXAFS for this sample. In contrast the Mo-K-edge data for **1** are relatively insensitive to these solvation effects, as might be expected if the Mo–Bi bonds are essentially unaffected by dissolution.

For complex **5** the Bi-L_{III} EXAFS interatomic distances are in reasonable agreement with the crystallographic values [Bi–Fe 2.689(2), Bi–Cl 2.939(4) and 3.077(9) Å,[6] *cf.* Bi–Fe mean 2.687(7), Bi–Cl 2.84(2), 2.98(3) Å] although the Bi–Cl distances are *ca.* 0.1 Å larger than X-ray values. Also fitted was the Bi···Bi distance which is strongly indicative of a cyclic oligomeric structure for **5** [Bi···Bi 3.985(12), *cf.* mean 3.97 Å

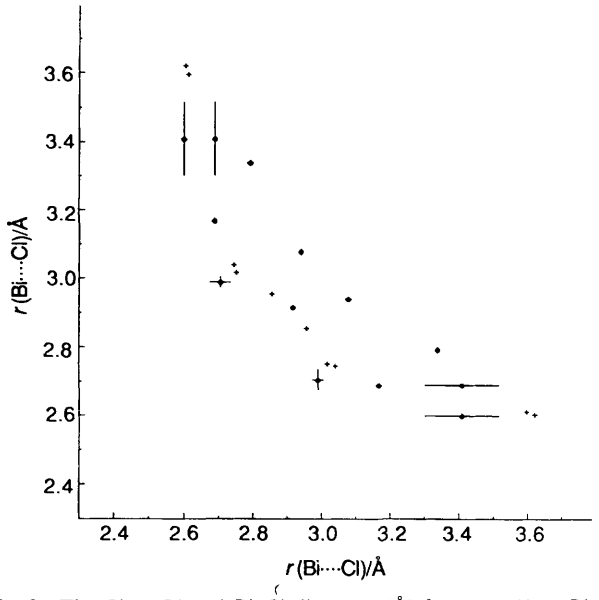

Fig. 9 The Cl · · · Bi and Bi–Cl distances (Å) for *trans*-Cl · · · Bi–Cl bonds in $[BiCl(ML_y)_2]$ complexes determined by crystallography (+) and EXAFS (⊕)

by crystallography]. In marked contrast the Bi · · · Bi distances in linear chain polymers (as in crystalline **1** and **2**) are *ca.* 5.5 Å. The Fe-K-edge data for **5** are in reasonable agreement with both the Bi-L_{III} EXAFS and the crystallographic values [Fe–Bi 2.685(5), Fe–C(O) 1.750(6), Fe–$C(C_5H_5)$ 2.106(6), Fe · · · O 2.915(5) and Fe · · · Fe 4.32(1) Å]. The latter dimension implies an Fe–Bi–Fe angle of 107(1)° in good agreement with the crystal structure values [109.7(1)–110.0(1)°]. The effects of solvation on the EXAFS spectra and model fitting for **5** are broadly similar to those for **1** (and for $[BiCl\{Mn(CO)_5\}_2]$[4]). In summary, therefore, the Bi–Cl · · · Bi bridges are broken and the Cl · · · Bi contact replaced by a Bi–O(thf) contact. In this case the Bi · · · Bi contacts clearly fitted in solid **5** are absent (and unfittable) in the EXAFS for the thf solution of **5**.

For $BiCl_3$ **8** the effect of dissolution in thf on the EXAFS spectra is rather different from the pattern of behaviour established for **1** and **5** (see Fig. 8). The EXAFS is substantially higher in amplitude and similar in frequency for the solution state as compared with the solid. This may be understood by reference to the solid-state crystal structure[7] which shows quite variable Bi–Cl distances (2.468–2.518, mean 2.500 Å) and a range of five longer Bi · · · Cl interactions (3.216–3.450 Å). In the absence of such secondary interactions (as, *e.g.*, in solution) one might imagine that rather shorter and more regular primary Bi–Cl bond lengths would result. Such a picture is consistent with the observed Bi–Cl distances and Debye–Waller factors [solid 2.505(4), a = 0.015(2) $Å^2$; solution 2.489(1), a = 0.008(1) $Å^2$]. No successful fits of Bi–O contacts were possible for these solution data. This may reflect rather diffuse and irregular bonding of thf to $BiCl_3$ in this solution. In this context we note the wide range of Bi · · · O(ether) distances observed by crystallography for a $BiCl_3$ complex of 18-crown-6 (1,4,7,10,13,-16-hexaoxacyclooctadecane) (Bi · · · O 2.77–3.16 Å).[8] Also of note in that crystal structure is the presence of a Bi–OH_2 contact [2.50(3) Å] and the average Bi–Cl distance [2.503(11) Å]. The latter is close to our EXAFS-determined Bi–Cl distances for $BiCl_3$ in both solid and solution phases. The relative shortness of the Bi–OH_2 contact might imply that the short Bi–O distances observed for thf solutions of **1** and **5** above could result from water contamination of these solutions. This is hard to rule out on the basis of the available data. All that can be said is that dried and degassed solvent was used, the samples were prepared and sealed in a glove-box and were stable over much longer periods than the EXAFS experiment (according to IR spectroscopy), there being no indication of the decomposition that would be expected if these solution samples did contain significant amounts of water. When deliberately wet thf (1 equivalent of H_2O per $BiCl_3$) was used the EXAFS spectra obtained were indistinguishable from those reported for $BiCl_3$ in Table 7, and a white precipitate was formed (presumably of BiOCl).

In the cases of complexes **2**, **6** and **7** the objective of the EXAFS studies was structure analysis of unknown solid-state structures, although in the event the crystal structure analysis of **2** was subsequently achieved (see above). Two sets of solid-state Bi-L_{III} and W-L_{III} EXAFS spectra were collected for **2**. The better-quality (as judged by reproducibility and signal to noise) data sets were collected for a sample that did *not* contain crystals of suitable quality for X-ray crystal structure analysis, and it is the analysis of these data that is presented in Table 7. The bonded distances (Bi–W, Bi–Cl, W–C, see Table 7) were much as to be expected and not dissimilar to the corresponding values for the molybdenum analogue, complex **1**. However a striking feature of the model fitted to the Bi-L_{III} EXAFS data is the presence of a Bi · · · Bi contact *ca.* 3.87 Å. As noted above this distance is characteristic of a cyclic trimer structure rather than the linear-chain form observed in the crystal structure of **2**. In contrast, for the poorer data collected for a crystalline sample of **2** (from which the crystal used for X-ray structure analysis was taken), no Bi · · · Bi distance <4.5 Å could be fitted (although the poor quality reduces the significance of this observation). Our *tentative* conclusion is that there may exist two solid forms of **2** one of which contains a cyclic oligomer (possibly a trimer) in addition to the form whose crystal structure is reported in this paper.

In the cases of complexes **6** and **7** the Bi-L_{III}-edge EXAFS data are dominated by the Bi–M (M = W or Mo) contribution at *ca.* 3.0 Å. The primary objective of the EXAFS study of **6** and **7** was the assessment of the co-ordination geometry at Bi (planar or pyramidal) as reflected in the M–Bi–M bond angles. The good agreement between EXAFS results and crystallography for such bond angles obtained for **1** and **5** indicates that such information is obtainable with care from the M (M = Fe or Mo) EXAFS data by triangulation of Bi–M and M · · · M distances. The major difficulty is in the reliable identification of the M · · · M contact, since such non-bonded distances are particularly prone to substantial distance variation which might drastically reduce their impact on the EXAFS data. In practice, features at distances corresponding to such contacts were observed for both **6** [W-L_{III} data, W · · · W fitted at 4.55(10) Å] and **7** (Mo-K data, Mo · · · Mo observed, but *not* significantly fitted, at *ca.* 4.2 Å). These distances correspond to M–Bi–M angles of 101(3) and 91° (unfitted) for **6** and **7** respectively. These values seem likely to be underestimates but also seem clearly to support a pyramidal geometry at Bi in both **6** and **7**. Other dimensions obtained from the EXAFS analyses (see Table 7) are as would be expected from crystallography.

(*iii*) Cl · · · Bi–Cl *Contacts.*—A graph of mutually *trans* Cl · · · Bi–Cl distances, determined from both crystallographic and EXAFS studies of $[BiCl(ML_y)_2]$ complexes, is shown in Fig. 9 (N.B. Cl–Bi–Cl >140° for all crystallographic data). A number of points emerge from this graph. First reasonable (but imperfect!) agreement between the two sources of data is visible. The general curvature of the plot is clear and may be taken to illustrate the effect of primary and secondary interactions on one another. Taking the Bürgi–Dunitz[9] view of such a plot, the distribution of points maps the S_N2 displacement of one chlorine by another in these formally three + one co-ordinate bismuth species. The form of this plot is broadly similar to those obtained for other associative nucleophilic substitution models studied in this way.[9] Thus the sum of Bi · · · Cl distances for the symmetrical intermediate geometry (where the two Bi–Cl distances are equal) is *ca.* 5.9 Å, *cf. ca.* 6.2 at the extremes of the plot for a highly asymmetric Cl · · · Bi–Cl system which models the initial stages of the substitution process. (A standard Bi–Cl

Table 8 Crystallographic data

Compound	**2**	**3**	**4**
Formula	$C_{16}H_{10}BiClO_6W_2$	$C_{16}H_{10}BiBrMo_2O_6$	$C_{16}H_{10}BiIMo_2O_6$
M	1820.8	779.0	826.0
Crystal system	Monoclinic	Monoclinic	Monoclinic
Space group	$P2_1/n$	$P2_1/n$	$P2_1/n$
a/Å	18.559(10)	18.551(2)	12.148(1)
b/Å	10.708(6)	10.950(2)	13.223(2)
c/Å	19.683(11)	10.866(3)	14.268(2)
β/°	104.29(6)	104.29(1)	114.01(1)
U/Å^3	3790.5	3910.6	2093.6
Z	8	8	4
D_c/g cm^{-3}	3.190	2.646	2.620
μ/mm^{-1}	21.78	12.24	11.00
F(000)	3216	2848	1496
Crystal size/mm	0.10 × 0.27 × 0.27	0.15 × 0.15 × 0.19	0.15 × 0.23 × 0.38
Maximum indices hkl	22, 12, 23	22, 13, 23	14, 15, 16
Transmission factors	0.007–0.040	0.085–0.140	0.096–0.142
Reflections measured	11 958	9390	4514
Unique reflections	6737	6860	3680
Observed reflections	4878	4705	3003
R_{int}	0.039	0.033	0.039
Weighting parameters A		−18, 489, −967, 13, 101, −1326	33, −54, 258, −72, 50, 48
Extinction parameter x	2.2(4) × 10^{-7}	6(2) × 10^{-8}	2.8(4) × 10^{-7}
R	0.078	0.040	0.030
$R' = (\Sigma w\Delta^2/\Sigma wF_o^2)^{\frac{1}{2}}$	0.101	0.037	0.032
Goodness of fit	1.05	1.09	1.12
No. of parameters	434	470	236
Mean, maximum shift/e.s.d.	0.007, 0.038	0.004, 0.020	0.001, 0.004
Maximum, minimum electron density/e Å^{-3}	4.5, −2.6	1.22, −1.11	0.96, −0.79

single bond value for this type of molecule is found in $[BiCl\{Mo(CO)_2(CNBu^t)(\eta\text{-}C_5H_5)\}_2]$ Bi–Cl 2.610(2) Å^2 which is monomeric with no close Bi • • • Cl intermolecular contacts.) Such behaviour has, in other cases, been interpreted in terms of conservation of total bond order.[9] Further discussion of the details of this system and related arylbismuth halide systems will be deferred to a later paper. We note, however, that the intermolecular Bi • • • Cl interactions are an example of the secondary bonding described by Alcock[10] and that the correlation between the primary and secondary Bi–Cl bond distances is fully consistent with the view that the acceptor orbitals on the bismuth centre, which give rise to its Lewis acidity, are Bi–Cl σ* orbitals.[3] This model also accounts for the approximately *trans* disposition of the chlorides with respect to the bismuth centre although, as we described in ref. 3, other factors may also influence this angle. Further studies on the structures of four-co-ordinate $[BiX_2(ML_n)_2]$ complexes, including the molecules described herein, will also be the subject of a future paper.

Experimental

For standard general procedures, see ref. 4.

Preparations.—Compound **2** was prepared as described in ref. 2. Dark red-purple X-ray-quality crystals were obtained by solvent diffusion of hexane into CH_2Cl_2 solutions of **2** at −30 °C over a period of days.

Compound **3** was prepared as described for **1**[2] but using $BiBr_3$. Typical yields of 90% were obtained and dark green X-ray-quality crystals were grown from thf–hexane mixtures at −30 °C. The infrared spectrum (thf solution, Nicolet 20 SXB FTIR spectrometer, CO stretching region) showed signals at 2009s, 1978m, 1969(sh) and 1909m cm^{-1}. The appearance of the spectrum is similar to that shown for **1** in thf in ref. 2.

Compound **4** was isolated from the reaction between $[Bi\{Mo(CO)_3(\eta\text{-}C_5H_5)\}_3]$ **7** and I_2 according to the following procedure. Samples of red **7** (0.154 g, 0.163 mmol) and purple iodine (0.041 g, 0.163 mmol) were combined as solids and dissolved in thf (15 cm^3). This resulted in a deep green solution which was stirred for 30 min after which time all volatiles were removed by vacuum. The crude solid was washed with hexane (5 × 15 cm^3) to remove $[MoI(CO)_3(\eta\text{-}C_5H_5)]$ then redissolved in fresh thf (10 cm^3) and filtered through Celite. The resulting dark green solution was layered with hexane (30 cm^3) and solvent diffusion over a period of days at −22 °C afforded shiny dark green crystals **4** (0.052 g, 39%). A second recrystallisation by the same method produced single crystals of **4** suitable for X-ray diffraction. Infrared: ν(CO) (thf) 2009s, 1979m and 1916m cm^{-1}, similar to **1** (Found: C, 23.5; H, 1.2. Calc. for $C_{16}H_{10}BiIMo_2O_6$: C, 23.3; H, 1.2%). NMR (CD_2Cl_2); ^{1}H, δ 5.50; ^{13}C-{^{1}H}, δ 94.0.

X-Ray Crystallography.—Crystallographic data are summarised in Table 8 for compounds **2**–**4**. Crystals were examined on a Stoe-Siemens diffractometer with graphite-monochromated Mo-Kα radiation (λ = 0.710 73 Å), at room temperature (295 K). Cell parameters were refined from 2θ values of 32 reflections in the range 20–25°, measured at ±ω. Intensities were measured in a ω–θ scan mode with on-line profile fitting.[11] In each case, the maximum 2θ was 50° and a complete unique set of data was collected (indices ±h, +k, +l), together with a partial set of equivalent reflections. Semiempirical absorption corrections were applied, and no significant change was observed in the intensities of three periodically monitored standard reflections.

The structures were determined from reflections with $F > 4\sigma_c(F)$, where σ_c was derived from counting statistics only. Compounds **2** and **3** are isostructural with **1**;[2] the known atomic coordinates of **1** were used for refinement of **3**, but the structure of **2** was actually solved independently from a Patterson synthesis and a different choice of asymmetric unit and origin was made. The heavy atoms of **4** were located by direct methods, and remaining atoms by difference syntheses. Refinement[12] was by blocked-cascade least-squares methods to minimise $\Sigma w\Delta^2$ with $\Delta = |F_o| - |F_c|$. The weighting scheme was $w^{-1} = \sigma_c^2(F) + 0.007\,31F^2$ for **2** and $w^{-1} = \sigma^2(F) = \sigma_c^2(F) +$

$A_1 + A_2G + A_3G^2 + A_4H + A_5H^2 + A_6GH$ for **3** and **4**, where $G = F_o/F_{max}$ and $H = \sin\theta/\sin\theta_{max}$.[13] Atomic scattering factors were taken from ref. 14. Non-hydrogen atoms were refined anisotropically; H atoms were constrained on ring-angle external bisectors, with C–H 0.96 Å, $U(H) = 1.2U_{eq}(C)$. For **2** the C_5H_5 rings were additionally constrained as ideal pentagons of side 1.420 Å. An isotropic extinction parameter x was refined, such that $F_c' = F_c/(1 + xF_c^2/\sin2\theta)^{\frac{1}{4}}$. The major features of residual difference syntheses were close to heavy atoms in each case.

EXAFS.—All EXAFS data were collected at the Daresbury Syncrotron Radiation Source (SRS) on station 7.1 in transmission mode, using samples prepared in a glove-box under nitrogen. Solid samples were typically of *ca.* 1 mm thickness and were diluted in boron nitride in order to achieve changes in $\log(I_0/I)$ in the range 1–2 at the absorption edge. Solution spectra were measured in cells of thickness *ca.* 3 mm and summed to provide the data to be analysed. Raw data were corrected for dark currents and converted to k-space (with EXCALIB[15]), and backgrounds subtracted (with EXBACK[15]) to yield EXAFS function $\chi^{obs}{}_i(k)$. These were Fourier filtered to remove features at distances below *ca.* 1.2 Å but *not* to remove long-distance features of the quasi-radial distribution function (*i.e.* no noise removal was attempted). Model fitting was carried out with EXCURV 90,[15] using curved-wave theory allowing for multiple scattering to third order for near-linear atom arrangements (M–C–O). Except where noted, only shells significant at the 99% level[16] were included in final models, *i.e.* shells added to the model caused reduction in the R indices by >6% of their previous value. Details of the final models employed are listed in Table 7, which gives interatomic distances (r_n), Debye–Waller factors (a_n) and the 'co-ordination' numbers (N), *i.e.* the numbers of atoms in a given shell *n*. *Ab initio* phase shifts and back-scattering factors using spherical wave theory with 25 *l* values were used throughout. The phase shift for chlorine in bismuth data was checked using fits to Bi-L_{III}-edge data for the compounds $[BiCl\{Mo(CO)_3(\eta\text{-}C_5H_5)\}_2]$ **1** and $BiCl_3$ **8** in the solid state. The calculated molybdenum phases, $\varphi(k)$, for the Bi-L_{III}-edge data were modified according to the equation $\varphi'(k) = (1.0 + bk)\varphi(k)$, where $b = -0.049(10)$, by refinement to obtain Bi–Mo distances in agreement with the X-ray crystal structure of **1**. The values used throughout for the proportion of absorption leading to EXAFS ('AFAC' = 0.8) and the magnitude of inelastic effects modelled by an imaginary potential ('VPI' = −4.0 eV, *ca.* -6.4×10^{-19} J), were confirmed for Bi-L_{III}-edge data by fits to **2** and **6** and for data at other edges by similar methods. Multiple scattering effects were allowed for in the cases of W, Mo and Fe data for the CO ligands.

Acknowledgements

We thank the SERC for financial support, the staff of the Daresbury SRS for technical support and BP Research (Sunbury) for CASE Awards (to N. A. C. and G. A. F.).

References

1 W. Clegg, N. A. Compton, R. J. Errington and N. C. Norman, *J. Chem. Soc., Dalton Trans.*, 1988, 1671.
2 W. Clegg, N. A. Compton, R. J. Errington, N. C. Norman, A. J. Tucker and M. J. Winter, *J. Chem. Soc., Dalton Trans.*, 1988, 2941.
3 W. Clegg, N. A. Compton, R. J. Errington, G. A. Fisher, D. C. R. Hockless, N. C. Norman and A. G. Orpen, *Polyhedron*, 1991, **10**, 123.
4 N. A. Compton, R. J. Errington, G. A. Fisher, N. C. Norman, P. M. Webster, P. S. Jarrett, S. J. Nichols, A. G. Orpen, S. E. Stratford and N. A. L. Williams, *J. Chem. Soc., Dalton Trans.*, 1991, 669.
5 P. Panster and W. Malisch, *J. Organomet. Chem.*, 1977, **134**, C32.
6 J. M. Wallis, G. Müller and H. Schmidbaur, *J. Organomet. Chem.*, 1987, **325**, 159.
7 S. C. Nyburg, G. A. Ozin and J. T. Szymanski, *Acta Crystallogr., Sect. B*, 1971, **27**, 2298.
8 M. G. B. Drew, D. G. Nicholson, I. Sylte and A. Vasudevan, *Inorg. Chim. Acta*, 1990, **171**, 11.
9 H. B. Bürgi and J. D. Dunitz, *Acc. Chem. Res.*, 1983, **16**, 153.
10 N. W. Alcock, *Adv. Inorg. Chem. Radiochem.*, 1972, **15**, 1.
11 W. Clegg, *Acta Crystallogr., Sect. A*, 1981, **37**, 22.
12 G. M. Sheldrick, SHELXTL, an integrated system for solving, refining, and displaying crystal structures from diffraction data, University of Göttingen, 1985, revision 5.
13 Wang Hong and B. E. Robertson, *Structure and Statistics in Crystallography*, ed. A. J. C. Wilson, Adenine Press, New York, 1985, p. 125.
14 *International Tables for X-Ray Crystallography*, Kynoch Press, Birmingham, 1974, vol. 4, pp. 99, 149.
15 EXCALIB, EXBACK and EXCURV 90, N. Binstead, S. J. Gurman and J. W. Campbell, SERC Daresbury Laboratory, 1990.
16 R. W. Joyner, K. J. Martin and P. Meehan, *J. Phys. C*, 1987, **20**, 4005.

Received 26*th June* 1991; *Paper* 1/03216J